COMMUNICATION

Template-Free Synthesis of Interconnected Hollow Carbon Nanospheres for High-Performance Anode Material in Lithium-Ion Batteries

Fu-Dong Han, Yu-Jun Bai, Rui Liu, Bin Yao, Yong-Xin Qi, Ning Lun, and Jian-Xin Zhang**

The ever-increasing demand for rechargeable batteries in some newly emerging portable electronic devices, advanced medical devices, and in particular, electric vehicles and hybrid electric vehicles has sparked research efforts in developing lithium ion batteries (LIBs) with high storage capacity and excellent rate performance.[1] Graphite, the mainstay of anode materials for commercialized LIBs, could hardly meet the demand because of its low theoretical specific capacity (372 mAh g^{-1}), and thus provides ample opportunity for exploring alternative high-performance electrode materials. Si, Sn, SnO_2 and some transition metal oxides with ultra high theoretical capacities have been considered due to their special mechanism for Li storage. Unfortunately, huge volume change (in alloying electrodes) and large voltage hysteresis (in conversion electrodes) occurring in these materials during Li insertion and extraction handicap their extensive applications.[2,3] Therefore, continual research has been focused on designing new carbon-based anodes with high performances by virtue of their favorable stability and outstanding kinetics. Up to date, large number of novel carbon-based electrode materials with various microstructures have been investigated, such as carbon nanobeads,[4] nanotubes,[5] nanofibers,[6] graphenes,[7] ordered mesoporous carbon,[8] hierarchically porous carbon,[9] and their composites.[10,11] Among these alternatives, hollow structured carbon materials (HSCMs) have been demonstrated to be attractive, since the unique hollow structure could facilitate Li^+ transport by offering a large surface area and a short diffusion distance.[12] In addition, HSCMs are sometimes used to address the capacity-fading problem of other anode materials with huge volume changes during the Li insertion and extraction, where the hollow carbon structures serve as barriers to suppress agglomeration of active particles and provide space for buffering volume expansion.[13–15] Up to now, only a few reports have been referred to the Li storage of HSCMs. For example, when crystalline carbon hollow spheres (750 nm) were used as anode materials in LIBs, a high rate capacity could be achieved due to the high electronic conductivity arising from the highly crystalline structure.[16,17] Nanographene-constructed hollow carbon spheres (380 nm) exhibited excellent performance for Li-ion storage owing to the comprehensive effect of the nanochannels arranging perpendicularly to the surface of hollow nanospheres and the interior graphitic solid walls.[18] However, most of HSCMs used in LIBs with comparable performance were prepared by complex methods involved templates and multiple synthetic steps, thus industrially unfavorable for continuous production on a large scale. Moreover, the large size of the materials inherited from the templates could not allow the capacity of the electrode materials to be fully achieved. Therefore, it is crucially important to develop a facile, economical and template-free method to synthesize HSCMs especially with the size in nanometer scale for high performance electrode materials.

In this work, we report a template-free method to synthesize interconnected hollow carbon nanospheres (HCNSs). Briefly, the HCNSs were simply prepared via pressure-assisted reduction and graphitization of sucrose in autoclaves, using Zn as a reductant. The obtained HCNSs with a high surface area, very thin graphitic shells and an interconnected structure exhibit excellent performances as the electrode material for LIBs. Importantly, the facile and economical preparation process is scalable to an industrially feasible approach.

Field-emission scanning electron microscopy (FESEM) and transmission electron microscopy (TEM) were used to examine the morphology and microstructure of the as-prepared HCNSs. From the FESEM image shown in **Figure 1**(a), the majority of the product exhibits spherical morphology with diameters ranging from 50 to 100 nm. A typical TEM image shown in Figure 1(b) reveals the hollow nature of the spheres. Compared with the HSCMs, the as-obtained HCNSs are interconnected, a distinct feature that will be favorable for the performance of HCNS electrode as discussed later.

From the high-resolution TEM (HRTEM) image shown in Figure 1(c), the shell of the HCNSs exhibits an almost uniform thickness of about 10 nm and a graphitic structure. Nevertheless, most of the graphene layers are discontinuous, and some isolated layers intercalate into the adjacent layers (as pointed out by arrows), giving rise to a large number of defects such as edges and pores. These unique microstructures are reasonably resulted from the low graphitization degree of the HCNSs due to the low preparation temperature (550 °C). The lattice spacing of 0.37 nm is larger than that of (002) plane for graphite (0.335 nm), and the expansion of *d*-spacing confirms the low graphitization degree of the as-obtained HCNSs. The broadening nature of the (002) diffraction peak in the XRD pattern (Figure S1) is another evidence for the low graphitization degree. Moreover, the graphitic structure of the HCNSs could be further supported by Raman spectroscopy (Figure S2). Two characteristic peaks around 1338 and 1590 cm^{-1} could be ascribed to D band arising from the defects and disorders in carbonaceous solid and G band from

F. D. Han, Prof. Y. J. Bai, R. Liu, B. Yao, Y. X. Qi, N. Lun, Prof. J. X. Zhang
Key Laboratory for Liquid–Solid Structural Evolution and Processing of Materials (Ministry of Education)
Shandong University
Jinan 250061, P. R. China
E-mail: byj97@126.com; jianxin@sdu.edu.cn

DOI: 10.1002/aenm.201100340

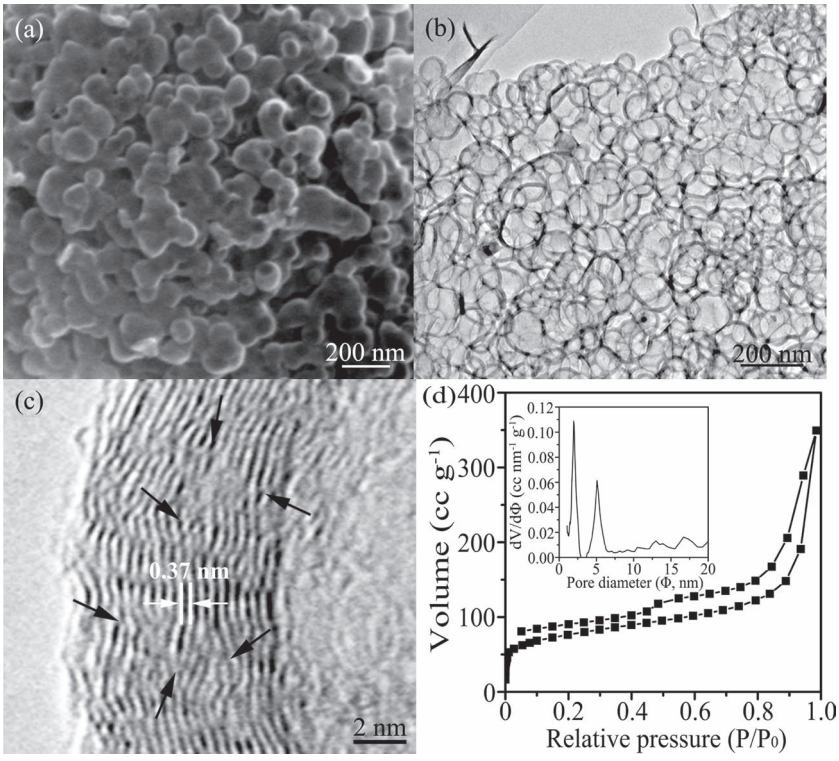

Figure 1. (a) FESEM image of the as-obtained HCNSs. (b) TEM image of the HCNSs. (c) HRTEM image of the shell, the black arrows show the intercalated layers present in the HCNSs. (d) Nitrogen adsorption/desorption isotherms and the corresponding pore-size distribution curve (inset) of the HCNSs.

the stretching mode of C-C bonds of typical graphite, respectively.[19] The intensity ratio (I_D/I_G) of the two bands is about 0.87, further verifying the low graphitization degree of the as-obtained HCNSs. The discontinuous graphene layers and the numerous defects in the shells of HCNSs are not only propitious to the Li-ion insertion and extraction but also to the diffusion of Li-ions, so it is expected that the HCNSs might exhibit excellent electrochemical performances.

The nitrogen absorption/desorption isotherms of the as-obtained HCNSs (Figure 1d) exhibit a typical IV-type curve. The specific surface area calculated with the Brunauer–Emmett–Teller model is 270 m^2 g^{-1}, and bimodal-pores with detectable sizes of 1.9 and 5.1 nm can be clearly distinguished from the pore size distribution curve (Inset of Figure 1d). These nanopores, also observed by HRTEM, are probably generated during the removal of the residual Zn and the byproduct of ZnO dispersed in the HCNSs or intercalated into the graphitic shells. In addition, some micropores could also be produced during the carbonization of the HCNSs.[20,21]

Electrochemical characteristics of the as-obtained HCNS electrode are presented in **Figure 2.** From the discharge (Li insertion)/charge (Li extraction) curves (Figure 2(a)) for

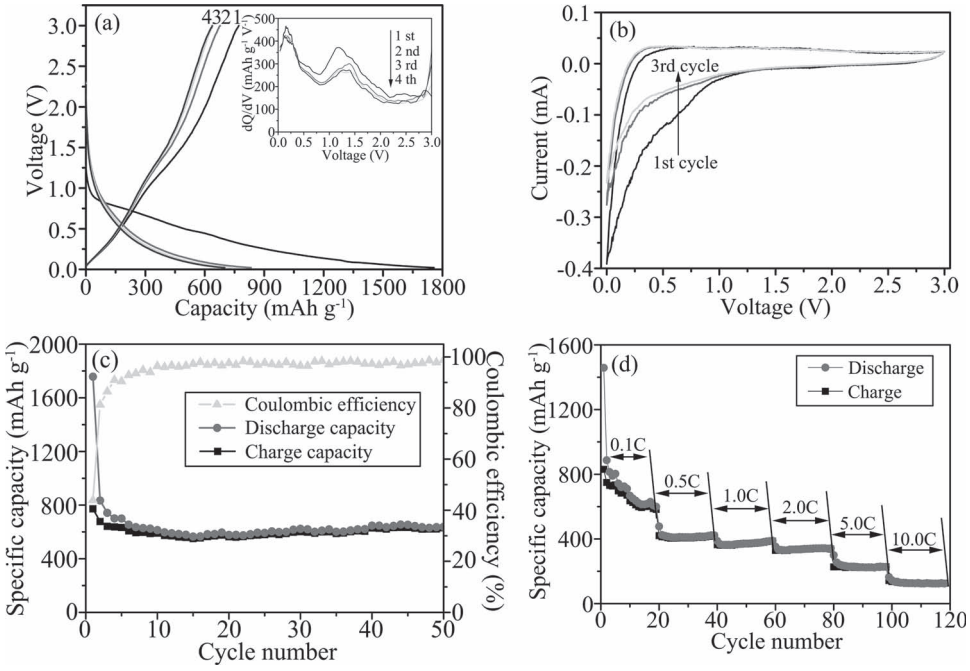

Figure 2. Electrochemical characteristics of the HCNS electrode. (a) Galvanostatic charge/discharge curves at a rate of C/10, (b) CV at a scan rate of 0.1 mV/s, (c) cycling performance at a rate of C/10, (d) rate performance at different rates. The inset in (a) shows the differential capacity versus cell voltage plots during charging of the electrode.

the first four cycles at a rate of C/10 (one Li per six formula units (LiC_6) in 10 h), the HCNS electrode delivers a reversible capacity as high as 772 mAh g^{-1} during the first cycle, which is about 108% higher than that of graphite and is also higher than those of other HSCMs.[16–18] Meanwhile, a large irreversible capacity of 985 mAh g^{-1} occurs in the electrode, which is a phenomenon to be expected in carbonaceous electrodes due to the formation of solid electrolyte interface (SEI) film on the surface of carbon and/or to the irreversible Li insertion into special positions such as the vicinity of residual H atoms.[22–24] Furthermore, the shape of the discharge and charge curves is similar to those previously reported for nano-sized carbonaceous materials.[5,18,23] In the first discharge process, the voltage drops rapidly with a plateau occurring in the region of 0.9-0.5 V (Figure 2(a)), while a large portion of specific capacity falls at the voltage below 0.5 V. By contrast, the charge curve extends steeply from about 0.02 to 3 V. The plateau in the first discharge process, which disappears from the next cycle, can be ascribed to the SEI formation on the HCNS surfaces. To specifically understand the Li storage in the HCNS electrode, the differential capacity versus cell-voltage plots for the first four charge processes are given in the inset of Figure 2(a). The two peaks at ~0.2 V and ~1.3 V and a slope from 2.7 to 3.0 V demonstrate that multiple Li storage positions are present in the as-obtained HCNSs. Accordingly, the peak at ~0.2 V can be attributed to the Li extraction from the graphitic layers, and the peak at ~1.3 V to the Li extraction from the defects in the HCNSs, such as pores, vacancies, edges and corners of the graphitic layers. As has been reported, the slope from 2.7 to 3.0 V is related to the heteroatoms (residual H) on the surface of HCNSs.[18,23,25,26]

The cyclic voltammograms (CV) of the HCNS electrode are shown in Figure 2(b), the shape of the CV curves matches well with the charge/discharge profiles. Figure 2(c) displays the cycling performance of the HCNS electrode examined under long-term cycling up to 50 cycles, revealing a good cyclic performance and reversibility. After 50 cycles, the electrode still maintains a specific reversible capacity of 630 mAh g^{-1}. Figure 2(d) shows the capacities at various charge/discharge rates. The cell was first cycled at 0.1 C for 20 cycles, followed by cycling with a stepwise increase of the discharge/charge rates to as high as 10 C. Reversible capacities of 409 mAh g^{-1} at the discharge/charge rate of 0.5 C, 373 mAh g^{-1} at 1 C, 337 mAh g^{-1} at 2 C, 229 mAh g^{-1} at 5 C, and 133 mAh g^{-1} at 10 C were achieved respectively, demonstrating the excellent rate performance of the HCNS electrode. Moreover, the excellent cycling performance increasing with rate is noteworthy, somewhat similar to what has been observed in hierarchically porous carbon monoliths.[9] The rate performance of the HCNSs is superior to that of the commercial natural graphite,[27] carbon nanobeads,[28] carbon nanotubes[11] and graphene[29], suggesting the advantage of the unique interconnected HCNSs in effectively improving the rate performance.

The highly reversible capacity, excellent cyclic performance and rate performance make the HCNSs a promising candidate as anode material for high-performance LIBs. Such pronounced electrochemical performance can be ascribed to the unique structure of the as-obtained HCNSs, as shown in **Figure 3**. First, the high surface area of the HCNSs provides a high electrode/electrolyte contact area and a large quantity of active sites for charge-transfer reactions, though a large irreversible capacity loss is concomitant as well. Second, the graphitic shells and the interconnected structure of the HCNSs ensure the fast and continuous transportation of electrons in the electrode, and the shell thickness of about 10 nm could also greatly reduce the solid-state transport lengths for Li diffusion, which are of great importance for the performance of the electrode materials. To support this viewpoint, we measured the electronic conductivity of the HCNSs employing a four-probe method by pressing the HCNSs into a thin plate, and the measured value is as high as 0.28 S cm^{-1}. In addition, the discontinuous graphene layers in the shells could facilitate not only the Li insertion and extraction but also the diffusion of Li, such a mechanism is similar to that long carbon nanotubes cutting into short segments could achieve enhanced performance.[5] Moreover, the larger *d*-spacing of the (002) plane could also result in an enhanced reversible capacity due to the facile intercalation/extraction of Li into the graphitic shells.[7] Finally, the nanopores (including micropores and mesopores), together with some other defects such as edges and vacancies in the as-obtained HCNSs could provide more lithium storage sites, contributing to the high reversible capacity of the HCNSs.[23] Meanwhile, these nanopores and the hollow structure itself may provide extra space for buffering the volumetric change (about 10% in graphite electrodes[26]) of the HCNS electrode during the Li insertion and extraction especially at high rates, beneficial to the stability of the electrode during long cycle operation.

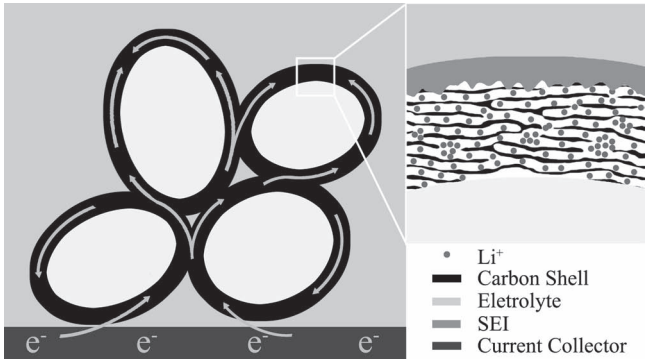

Figure 3. Schematic representation of Li storage in the HCNSs.

In conclusion, interconnected HCNSs could be simply prepared on large scale by pressure-assisted reduction and graphitization of sucrose in autoclaves. The HCNSs used as anode material for LIBs exhibit a large reversible capacity (630 mAh g^{-1} after 50 cycles), excellent cyclic performance and rate performance, highlighting the advantages of HSCMs for energy storage applications in high-performance LIBs. The high electrochemical performance of the HCNSs arises from their unique structure for facilitating rapid mass transport of electrons and Li ions and supplying multiple Li storage sites. The simple approach offers a new pathway for large-scale production of interconnected HCNSs for energy storage.

Experimental Section

Material Synthesis: The raw materials used are chemically pure zinc (Zn) and sucrose. Typically, Zn (23 g) and sucrose (7.8 g) were put into a

stainless steel autoclave of 30 mL capacity. The autoclave containing the raw materials was sealed tightly and heated in an electric oven to 550 °C, and maintained for 10 h at this temperature. When the autoclave was cooled naturally to ambient temperature, the product in the autoclave was collected and rinsed with dilute hydrochloric acid and deionized water, and then dried at 50 °C for 10 h. Black powders were ultimately obtained.

Material Characterization: The morphology of the product was examined using a Hitachi SU-70 field-emission scanning electron microscope and a JEOL JEM-2100 high-resolution transmission electron microscope. X-ray powder diffraction patterns were obtained on a Rigaku Dmax-rc diffractometer with Ni filtered Cu Kα radiation (V = 40 kV, I = 50 mA) at a scanning rate of 4°/min. Raman spectra were collected on a Lab-RAM HR800 with excitation from an argon ion laser (632.81 nm). Nitrogen adsorption and desorption isotherms were carried out at 77 K on a Quadrasorb SI sorption analyzer. The samples were degassed at 300 °C for 3 h under a vacuum in the degas port of the analyzer. The specific surface area was calculated with the Brunauer–Emmett–Teller (BET) model, and the pore-size distribution was calculated from the adsorption/desorption data by using the Density Functional Theory (DFT) method. The electronic conductivity of the HCNSs was measured employing a four-probe method (M123301) by pressing the HCNSs into a thin plate under a pressure of 18 Mpa in a mold of 13 mm in diameter.

Electrochemical Measurement: Electrochemical experiments were carried out in 2025 coin-type cells. The working electrodes were prepared by coating the slurry of HCNSs (80 wt%), carbon black (5 wt%), and polyvinylidene fluoride (PVDF) (15 wt%) dissolved in *n*-methyl pyrrolidinone (NMP) onto a Cu foil substrate and dried in a vacuum oven at 120 °C for 12 h. Li metal foil was utilized as the counter electrode, and Celgard 2300 was used as the separator. The electrolyte was composed of a solution of 1 M $LiPF_6$ in ethylene carbonate (EC) and dimethyl carbonate (DMC) (1:1 by volume). Half-cells were assembled in an argon-filled glove box. The cells were galvanostatically charged and discharged in the voltage range from 0.02 V to 3 V (versus Li/Li^+) at different current densities at room temperature. Cyclic voltammetry measurements were carried out on an electrochemistry workstation (PARSTAT 2273) over the potential range 0–3 V vs. Li/Li^+ at the scan rate of 0.1 mV s^{-1}.

Supporting Information

Supporting Information is available from the Wiley Online Library or from the author.

Acknowledgements

This work was supported by the National Natural Science Foundation of China (50972076, and 50872072), Shandong Provincial Natural Science Foundation, China (Y2008F26 and Y2008F40), Science and Technology Development Project of Shandong Province (2009GG10003001), and Special Fund for Postdoctoral Innovative Project of Shandong Province (200702024).

Received: June 22, 2011
Published online: August 19, 2011

[1] G. A. Nazri, G. Pistoia, *Lithium Batteries: Science and Technology*, Springer Science + Business Media, New York, **2009**.
[2] M. R. Palacín, *Chem. Soc. Rev.* **2009**, *38*, 2565.
[3] J. Cabana, L. Monconduit, D. Larcher, M. R. Palacín, *Adv. Mater.* **2010**, *22*, E170.
[4] H. Y. Wang, T. Abe, S. Maruyama, Y. Iriyama, Z. Ogumi, K. Yoshikawa, *Adv. Mater.* **2005**, *17*, 2857.
[5] X. X. Wang, J. N. Wang, H. Chang, Y. F. Zhang, *Adv. Funct. Mater.* **2007**, *17*, 3613.
[6] S. H. Yoon, C. W. Park, H. J. Yang, Y. Korai, I. Mochida, R. T. K. Baker, N. M. Rodriguez, *Carbon* **2004**, *42*, 21.
[7] E. J. Yoo, J. Kim, E. Hosono, H. S. Zhou, T. Kudo, I. Honma, *Nano Lett.* **2008**, *8*, 2277.
[8] H. S. Zhou, S. M. Zhu, M. Hibino, I. Honma, M. Ichihara, *Adv. Mater.* **2003**, *15*, 2107.
[9] Y. S. Hu, P. Adelhelm, B. M. Smarsly, S. Hore, M. Antonietti, J. Maier, *Adv. Funct. Mater.* **2007**, *17*, 1873.
[10] J. Zhang, Y. S. Hu, J. P. Tessonnier, G. Weinberg, J. Maier, R. Schlogl, D. S. Su, *Adv. Mater.* **2008**, *20*, 1450.
[11] Z. J. Fan, J. Yan, T. Wei, G. Q. Ning, L. J. Zhi, J. C. Liu, D. X. Cao, G. L. Wang, F. Wei, *ACS nano* **2011**, *5*, 2787.
[12] J. Liu, D. F. Xue, *Nanoscale Res. Lett.* **2010**, *5*, 1525.
[13] W. M. Zhang, J. S. Hu, Y. G. Guo, S. F. Zheng, L. S. Zhong, W. G. Song, L. J. Wan, *Adv. Mater.* **2008**, *20*, 1160.
[14] K. T. Lee, Y. S. Jung, S. M. Oh, *J. Am. Chem. Soc.* **2003**, *125*, 5652.
[15] F. Li, Q. Q. Zou, Y. Y. Xia, *J. Power Sources* **2008**, *177*, 546.
[16] Y. Wang, F. B. Su, J. Y. Lee, X. S. Zhao, *Chem. Mater.* **2006**, *18*, 1347.
[17] F. B. Su, X. S. Zhao, Y. Wang, L. K. Wang, J. Y. Lee, *J. Mater. Chem.* **2006**, *16*, 4413.
[18] S. B. Yang, X. L. Feng, L. J. Zhi, Q. Cao, J. Maier, K. Müllen, *Adv. Mater.* **2010**, *22*, 838.
[19] J. Robertson, *Mater. Sci. Eng., R.* **2002**, *37*, 129.
[20] F. Zhang, K. X. Wang, G. D. Li, J. S. Chen, *Electrochem. Commun.* **2009**, *11*, 130.
[21] W. Li, F. Zhang, Y. Q. Dou, Z. X. Wu, H. J. Liu, X. F. Qian, D. Gu, Y. Y. Xia, B. Tu, D. Y. Zhao, *Adv. Energy Mater.* **2011**, *1*, 382.
[22] S. Flandrois, B. Simon, *Carbon* **1999**, *37*, 165.
[23] N. A. Kaskhedikar, J. Maier, *Adv. Mater.* **2009**, *21*, 2664.
[24] T. P. Kumar, T. S. D. Kumari, A. M. Stephan, *J. Indian Inst. Sci.* **2009**, *89*, 393.
[25] S. B. Yang, J. P. Huo, H. H. Song, X. H. Chen, *Electrochim. Acta* **2008**, *53*, 2238.
[26] D. S. Su, R. Schlogl, *ChemSusChem*, **2010**, *3*, 136.
[27] P. Adelhelm, Y. S. Hu, L. Chuenchom, M. Antonietti, B. M. Smarsly, J. Maier, *Adv. Mater.* **2007**, *19*, 4012.
[28] J. C. Chang, Y. F. Tzeng, J. M. Chen, H. T. Chiu, C. Y. Lee, *Electrochim. Acta* **2009**, *54*, 7066.
[29] H. B. Wang, C. J. Zhang, Z. H. Liu, L. Wang, P. X. Han, H. X. Xu, K. J. Zhang, S. M. Dong, J. H. Yao, G. L. Cui, *J. Mater. Chem.* **2011**, *21*, 5430.